JPE 16-4-13

http://dx.doi.org/10.6113/JPE.2016.16.4.1367
ISSN(Print): 1598-2092 / ISSN(Online): 2093-4718

An Enhanced Finite-Settling-Step Direct Torque and Flux Control (FSS-DTFC) for IPMSM Drives

Sehwan Kim* and Jul-Ki Seok†

*,†Power Conversion Lab., Dept. of Electrical Eng., Yeungnam University, Gyeongsan, Korea

Abstract

This paper presents a discrete-time version of voltage and current limited operation using an enhanced direct torque and flux control method for interior permanent magnet synchronous motor (IPMSM) drives. A command voltage vector for airgap torque and stator flux regulation can be uniquely determined by the finite-settling-step direct torque and flux control (FSS-DTFC) algorithm under physical constraints. The proposed command voltage vector trajectories can be developed to achieve the maximum inverter voltage utilization for the discrete-time current limit (DTCL)-based FSS-DTFC. The algorithm can produce adequate results over a number of the potential secondary upsets found in the steady-state current limit (SSCL)-based DTFC. The fast changes in the torque and stator flux linkage improve the dynamic responses significantly over a wide constant-power operating region. The control strategy was evaluated on a 900W IPMSM in both simulations and experiments.

Key words: Discrete-time current limit (DTCL), Finite-settling-step direct torque and flux control (FSS-DTFC), Maximum inverter voltage utilization, Steady-state current limit (SSCL)

I. INTRODUCTION

Direct torque and flux control (DTFC) methods have been widely developed for high performance ac motor drives [1]-[4]. Recently, discrete-time versions of the DTFC, called the deadbeat-direct torque and flux control (DB-DTFC), have been introduced to achieve the fastest torque and flux response within operating limits [4], [5]. The DB-DTFCs apply the principle of deadbeat control to achieve a desired value in one inverter switching period. DB-DTFC methods have been implemented for IM drives [1], [2] and IPMSM drives [4]-[6]. However, in these studies, insufficient information was available to determine the stator voltage vector during a wide range of operation at elevated speeds.

When a command output voltage encounters a voltage limit due to elevated rotor frequencies or large torque changes, the controller requires a feasible command voltage to follow a desired value in a finite settling step. Recently, a finite-settling-step DTFC (FSS-DTFC) method associated with the inverter voltage and current constraints for IPMSMs has been proposed [5], [6]. The FSS-DTFC is an exact counterpart of the DB-DTFC, in terms of the physical constraints, in discrete time. The FSS-DTFC can be a suitable solution during voltage and current constrained operations. Here, the intersection of a current limited ellipse and a rotating hexagon becomes a feasible voltage vector in the next sampling instant. The fastest rate of torque changes can be achieved by scaling the voltage vectors on the hexagonal voltage boundary to ensure stator flux linkage regulation while meeting flux-weakening requirements. A natural transition from the maximum torque per ampere (MTPA) to the flux weakening mode is possible via a voltage selection rule. Therefore, the whole motor controller can be designed under a single control law, which leads to a reduction of the time and effort required for calibration of the controller over the entire operating space.

The aforementioned FSS-DTFC has many benefits. Howeveer, it has one important caveat because it relies on the steady-state current limit (SSCL) [5]-[7]. Although a relatively simple calculation can be achieved when using the SSCL, the number of potential secondary upsets is increased, i.e. a more complicated voltage selection rule due to multiple solutions, add-on harmonic production [5] which is more significant at higher speeds, and an instantaneous over-current exceeding the inverter maximum current.

In this paper, an enhanced FSS-DTFC method is proposed

Manuscript received Nov. 9, 2015; accepted Mar. 30, 2016
Recommended for publication by Associate Editor Shihua Li.
†Corresponding Author: doljk@ynu.ac.kr
Tel: +82-53-810-2484, Fax: +82-53-810-4767,Yeungnam University
*Department of Electrical Engineering, Yeungnam University, Korea

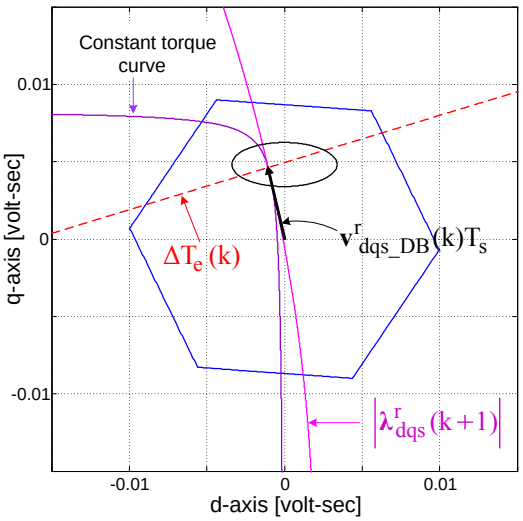

Fig. 1. Graphical solution in the non-limited region ($\omega_r = 0.6\omega_b$).

as an alternative SSCL-based FSS-DTFC using the discrete-time version of physical constraints. A unique command voltage trajectory has been sought at each discrete time step by genuine sampling-based knowledge, while the DB-DTFC is carried out under non-limited conditions. The successful application of this control approach was corroborated by graphical and analytical analyses that naturally led to a single voltage selection policy for the discrete-time current limit (DTCL)-based FSS-DTFC. The proposed DTCL-based FSS-DTFC uses an estimated stator current rather than the measured current to enhance the inverter reliability. The algorithm solves the drawbacks in terms of the number of potential secondary upsets encountered in the SSCL-based DTFC. The proposed method also provides direct manipulation of the stator flux linkage while utilizing the maximum inverter voltage in the voltage and current limited region.

II. Principle of DB-DTFC Under Non-Limited Condition

A DB controller is a special type of FSS controller where instead of achieving a desired response over multiple time periods, the response is achieved in one time step. The DB-DTFC is a high performance control technique where the torque and stator flux are independently controlled at the switching level under non-limited voltage conditions. Here, the inverse system model can be used to calculate a desired voltage vector for the next sample period in order to achieve the commanded air-gap torque and stator flux magnitude.

Fig. 1 shows a graphical representation of the stator voltage solutions in the synchronous d-q Volt-sec plane under the based speed. The desired change in torque [4], [5], $\Delta T_e(k)$, forms a dotted line in the complex stator Volt-sec plane and is shown in red. The stator flux linkage $|\lambda^r_{dqs}(k)|$ forms a large circle which is shown in pink. The voltage vector, which falls inside the voltage limits, was chosen as a feasible solution, $\mathbf{v}^r_{dqs\_DB}(k)T_s$, because it is the only achievable voltage in the next sampling time. This indicates that a smooth and fast response for the torque and stator flux can be achieved via the DB-DTFC in a single step under non-limited voltage conditions.

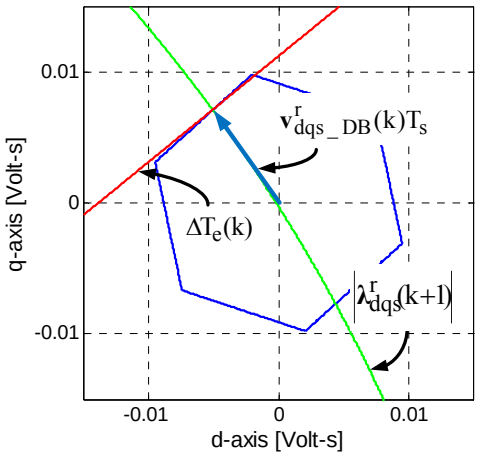

Fig. 2. Feasible solution at base speed ($\omega_r = \omega_b$).

III. Discrete-Time Physical Limits-Based Enhanced FSS-DTFC

When the motor speed rises, the deadbeat command voltage vector (labeled $\mathbf{v}^r_{dqs\_DB}(k)T_s$) approaches the hexagon-shaped voltage limit boundary, as shown in Fig. 2. The flux weakening operation starts on this boundary, where the speed is called the base speed (ω_b)).

Above the base speed, $\mathbf{v}^r_{dqs\_DB}(k)T_s$ is located outside the voltage limit. In this operation, the command voltage vector needs to be scaled back due to physical limits. For full utilization of the physical resources, both the voltage and current constraints should be considered when modifying the command voltage vector [5].

The stator current at the next sample time will exist on the current limit as:

$$i^r_{ds}(k+1)^2 + i^r_{qs}(k+1)^2 = I^2_{s\,max} \quad (1)$$

where $I_{s\,max}$ represents the maximum current limited by the inverter current rating. The modified voltage will be on the rotating hexagon voltage limit in the d-q Volt-sec plane. The FSS-DTFC suggests that the intersection of the current limited ellipse and the rotating hexagon becomes a feasible voltage vector in the next sampling instant [5]-[7].

The ac motor voltage and stator flux linkage equation in

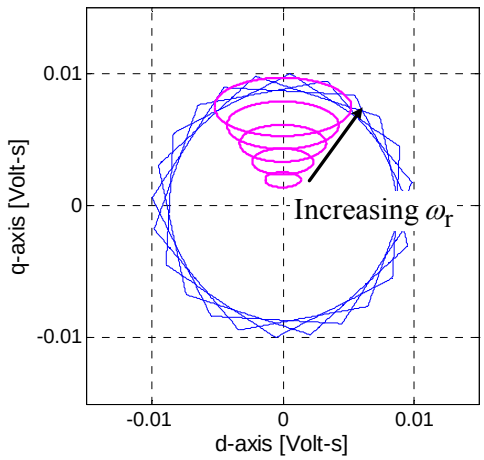

Fig. 3. SSCL trajectories with the rotor speed.

the rotor reference frame can be written in the following discrete time form:

$$\begin{aligned} v_{ds}^{r}(k) &= R_s i_{ds}^{r}(k) + \frac{L_d i_{ds}^{r}(k+1) - L_d i_{ds}^{r}(k)}{T_s} - \omega_r \lambda_{qs}^{r}(k) \\ v_{qs}^{r}(k) &= R_s i_{qs}^{r}(k) + \frac{L_q i_{qs}^{r}(k+1) - L_q i_{qs}^{r}(k)}{T_s} + \omega_r \lambda_{ds}^{r}(k) \end{aligned} \quad (2)$$

$$\begin{aligned} \lambda_{ds}^{r}(k) &= L_d i_{ds}^{r}(k) + \lambda_{pm} \\ \lambda_{qs}^{r}(k) &= L_q i_{qs}^{r}(k) \end{aligned} \quad (3)$$

where $\mathbf{v}_{dqs}^{r}(k)$ and $\mathbf{i}_{dqs}^{r}$ represent the d-q axis stator voltage and current vector in the rotor reference frame, respectively, and P denotes the number of poles. L_{dq} indicates the d-q axis inductance, λ_{pm} is the flux linkage of the PM, R_s is the stator resistance, and ω_r is the rotor angular velocity.

A. *Problem Statements of the SSCL-based FSS-DTFC*

At high speeds, the stator voltage can be simplified as:

$$\begin{aligned} v_{ds}^{r}(k) &\cong -\omega_r \lambda_{qs}^{r}(k) \\ v_{qs}^{r}(k) &\cong \omega_r \lambda_{ds}^{r}(k) \end{aligned} \quad (4)$$

By combining (1), (3), and (4), the SSCL can be described as an ellipse in the d-q Volt-sec plane:

$$\left(\frac{v_{ds}^{r}(k) T_s}{\omega_r L_q T_s} \right)^2 + \left(\frac{v_{qs}^{r}(k) T_s - \omega_r \lambda_{pm} T_s}{\omega_r L_d T_s} \right)^2 = I_{s\max}^2 . \quad (5)$$

Note that (5) moves in the positive q-axis direction with increasing speed, as shown in Fig. 3. In the SSCL-based FSS-DTFC method, a modified stator Volt-sec solution on the associated rotating hexagon boundary can be uniquely selected, while weakening the motor flux at a given rotor speed [5].

However, at higher speeds, the raised SSCL ellipse may cause two adjacent points that satisfy the torque generation requirements, as shown in Fig. 4(a) (~170% of ω_b in the testing motor). The choice of which point to use as a new command voltage vector is made by developing an additional voltage selection rule to meet the particular flux weakening requirement for the next sampling instant. In addition, Volt-sec solutions start vanishing from 170% of ω_b, as shown in Fig. 4(b).

Moreover, due to the fluctuating trajectories of the selected intersection, a command voltage progressively includes a certain amount of harmonics with multiples of six times the fundamental frequency with increasing rotor speeds [5]. These add-on harmonics may create unnecessary losses and can lead to unwanted mechanical vibrations.

The SSCL-based FSS-DTFC is penalized due to the instantaneous over-current that is not bounded within $I_{s\max}$, because the SSCL is only valid at the steady-state. Fig. 5 presents a simulation of the current magnitude waveform of the SSCL-based FSS-DTFC operation when $I_{s\max}$ is set to 4 A, which is the maximum motor current in a real system. Here, the harmonics and ripples from the PWM inverter operation were ignored to investigate the stator current characteristics staying on the current boundary.

This makes it very challenging to design and protect the inverter from over-current trips. These secondary upsets provide a compelling impetus to seek out an enhanced FSS-DTFC strategy a for more reliable and straightforward ac motor control.

B. *Principle of the DTCL-Based Enhanced FSS-DTFC*

Here, the purpose is to build a genuine discrete-time-based FSS-DTFC when physical limits are encountered. Equation (2) can be rewritten as:

$$\begin{aligned} L_d i_{ds}^{r}(k+1) &= v_{ds}^{r}(k) T_s + \alpha \\ L_q i_{qs}^{r}(k+1) &= v_{qs}^{r}(k) T_s + \beta \end{aligned} \quad (6)$$

where $\alpha = -R_s i_{ds}^{r}(k) T_s + L_d i_{ds}^{r}(k) + \omega_r \lambda_{qs}^{r}(k) T_s$ and $\beta = -R_s i_{qs}^{r}(k) T_s + L_q i_{qs}^{r}(k) - \omega_r \lambda_{ds}^{r}(k) T_s$. Then, the stator flux linkage becomes:

$$\begin{aligned} \lambda_{ds}^{r}(k+1) &= v_{ds}^{r}(k) T_s + \lambda_{pm} + \alpha \\ \lambda_{qs}^{r}(k+1) &= v_{qs}^{r}(k) T_s + \beta \end{aligned} \quad (7)$$

The DTCL can be obtained by combining (1), (6), and (7) as:

$$\left(\frac{v_{ds}^{r}(k) T_s + \alpha}{L_d} \right)^2 + \left(\frac{v_{qs}^{r}(k) T_s + \beta}{L_q} \right)^2 = I_{s\max}^2 \quad (8)$$

which forms the large ellipse in pink, at the base speed, shown in Fig. 6(a). Fig. 6(b) shows a zoomed snapshot near the hexagon of Fig. 6(a) with the rotor speed elevation. The

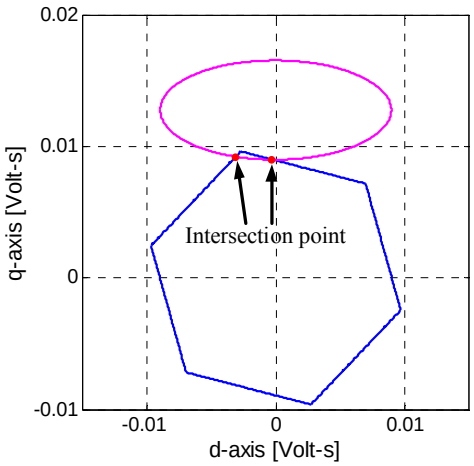

(a) Multiple points occurrence.

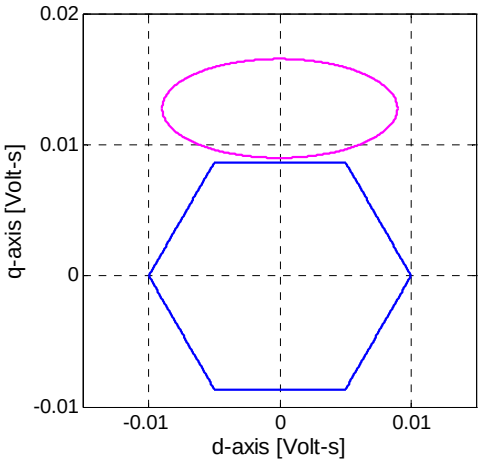

(b) Nonexistence of Volt-sec solution.

Fig. 4. The SSCL-based FSS-DTFC voltage selection at high speeds.

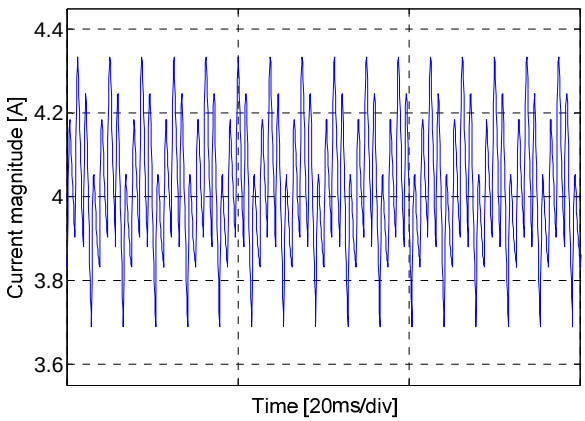

Fig. 5. The instantaneous over-current.

ellipse origin shifts upward as the rotor speed increases. An examination of whether the DTCL ellipse changes the Volt-sec solution trajectory significantly, when compared to that of the SSCL, would be an interesting subject.

The corresponding ellipse shape guarantees a unique Volt-sec solution for achieving a desired torque up to the theoretical maximum rotor speed, while satisfying the flux weakening requirements. This means that no additional voltage selection rules are required for multiple intersections in the entire operating range. In addition, the intersection trajectories stay in a considerably low fluctuation interval on the horizontal axis of the synchronous d-q Volt-sec plane, which suggests that no add-on harmonics appear in the command voltage vector. The stator current is bounded within $I_{s\max}$, as shown in Fig. 7, because the enhanced FSS-DTFC is performed based on discretized current constraints. This offers significant benefits in terms of inverter protection over the SSCL-based DTFC.

A selected voltage vector at the intersection of the DTCL ellipse and the rotating hexagon boundary can be obtained as follows:

$$v^r_{ds\_FSS}(k) = \frac{-\beta_d - \sqrt{\beta_d^2 - 4\alpha_d\gamma_d}}{2\alpha_d T_s}$$
$$v^r_{qs\_FSS}(k) = M_n v^r_{ds}(k) + \frac{B_n}{T_s} \quad (9)$$

where $\alpha_d = (L_q)^2 + (M_n L_d)^2$,

$\beta_d = 2\alpha(L_q)^2 + 2M_n(B_n + \beta)(L_d)^2$,

and $\gamma_d = (\alpha L_q)^2 + (B_n + \beta)^2 (L_d)^2 - (L_d L_q I_{s\max})^2$.

The boundary of each rotating hexagon sector can be modeled as a straight line in the d-q Volt-sec plane [5].

$$v^r_{qs}(k)T_s = M_n v^r_{ds}(k)T_s + B_n \quad (10)$$

where M_n and B_n are constant values given by the boundary of each hexagon sector.

In practice, the inevitable measurement and switching noise of $\mathbf{i}^r_{dqs}(k)$ can cause fluctuations of the DTCL trajectory in (8). Therefore, using an estimated current from a closed loop stator current observer [4]-[6] is desirable for avoiding the ringing associated with current noises as:

$$\left(\frac{v^r_{ds}(k)T_s + \hat{\alpha}}{L_d}\right)^2 + \left(\frac{v^r_{qs}(k)T_s + \hat{\beta}}{L_q}\right)^2 = I^2_{smax} \quad (11)$$

where:

$\hat{\alpha} = -R_s \hat{i}^r_{ds}(k)T_s + L_d \hat{i}^r_{ds}(k) + \omega_r \hat{\lambda}^r_{qs}(k)T_s$ and

$\hat{\beta} = -R_s \hat{i}^r_{qs}(k)T_s + L_d \hat{i}^r_{qs}(k) - \omega_r \hat{\lambda}^r_{ds}(k)T_s$.

The superscript "^" represents the corresponding variables that are estimated.

Fig. 8 shows an overall block diagram of the control system with the proposed enhanced FSS-DTFC algorithm. A discrete time Gopinath-style stator flux linkage observer is integrated into the enhanced FSS-DTFC system and is an

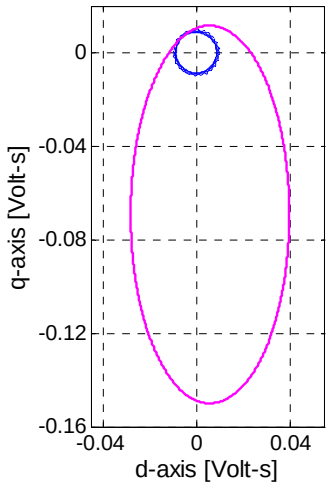

(a) DTCL trajectory at the base speed.

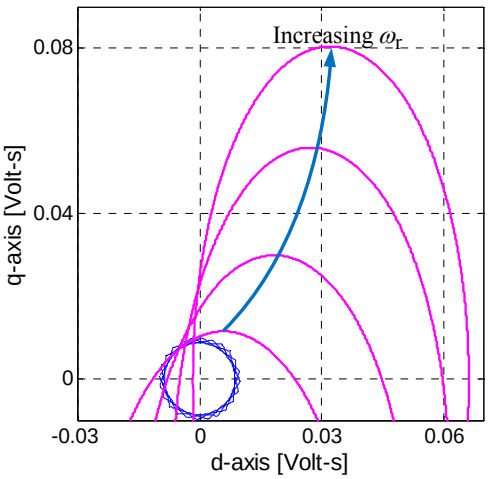

(b) DTCL trajectories with the rotor speed.

Fig. 6. DTCL-based FSS-DTFC voltage selection at high speeds.

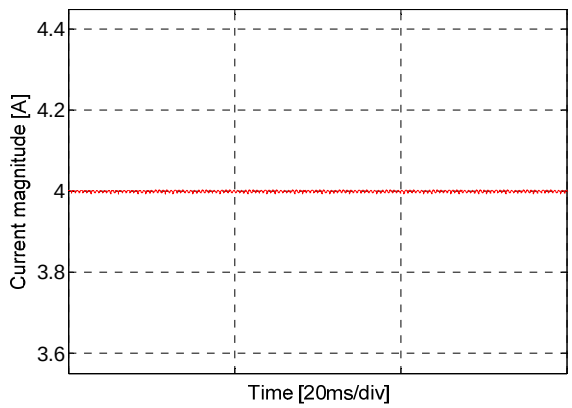

Fig. 7. Stator current magnitude of the enhanced FSS-DTFC.

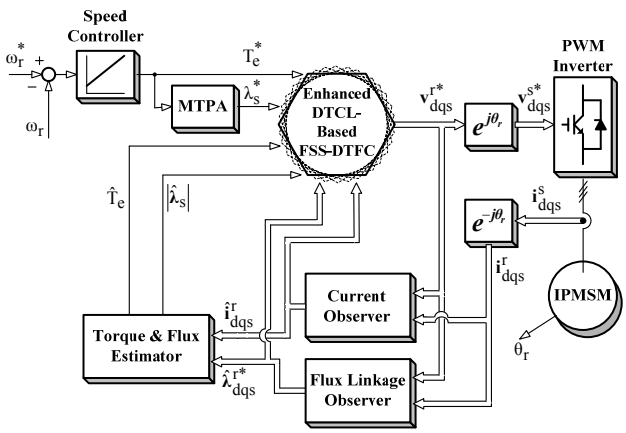

Fig. 8. Proposed DTCL-based DTFC strategy.

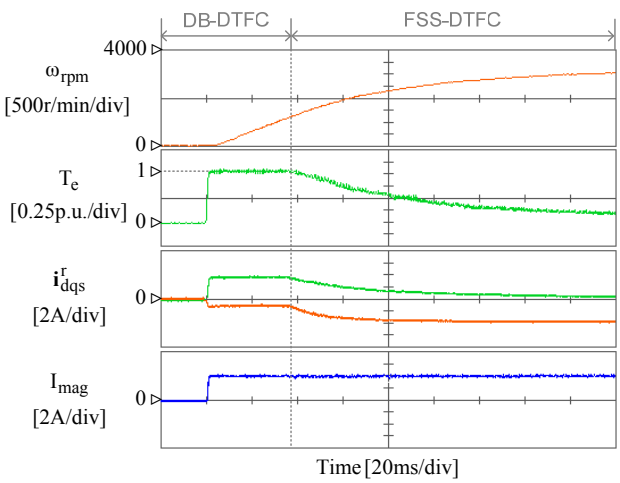

Fig. 9. Test results of the proposed enhanced DTFC.

important part for estimating the stator flux linkage [4]-[6]. For the stator flux linkage observer, the cross-coupling is decoupled when the stator current observer is developed.

IV. Experimental Results

The proposed DTCL-based FSS-DTFC algorithm was implemented on a 900 W IPMSM, as described in Table I. A 2500-pulse-per-revolution encoder was mounted on one end of the test motor to measure the actual position. A fixed MTPA curve was implemented to utilize both the electromagnetic and reluctance torques available in the IPMSM below the base speed [8]. The algorithm was implemented in an inverter with a constant PWM switching frequency of 5 kHz. Multidimensional map data tables were prepared to achieve accurate torque control based on steady-state measurements of the motor physical quantities [9], [10]. The stator current observer was designed in the rotor reference frame and its bandwidth was set to 200 Hz.

Test results in the motoring operation are depicted in Fig. 9, where the rotor speed, air-gap torque, measured d-q stator current, and stator current magnitude are illustrated from top to bottom. Here, the advent of flux weakening occurs at around 1300 r/min (t ≈ 58 ms) and I_{smax} is set as 4 A. The waveform of the air-gap torque shows that a smooth transition occurs between the DB-DTFC and the FSS-DTFC.

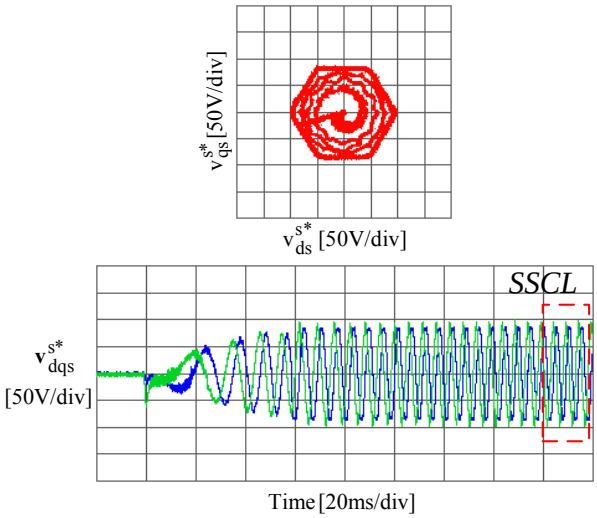

(a) Selected d-q command voltage waveforms.

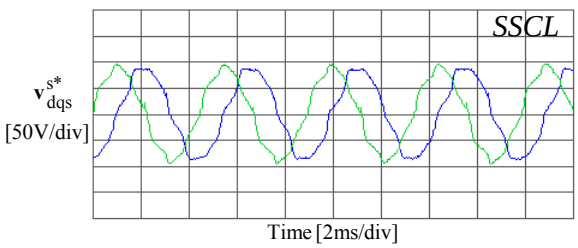

(b) Zoomed waveform of Fig. 10(a).

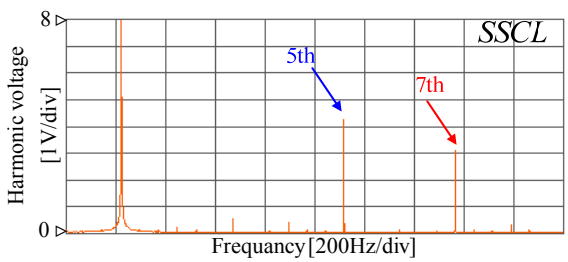

(c) FFT spectrum.

Fig. 10. Voltage waveforms of the SSCL-based FSS-DTFC.

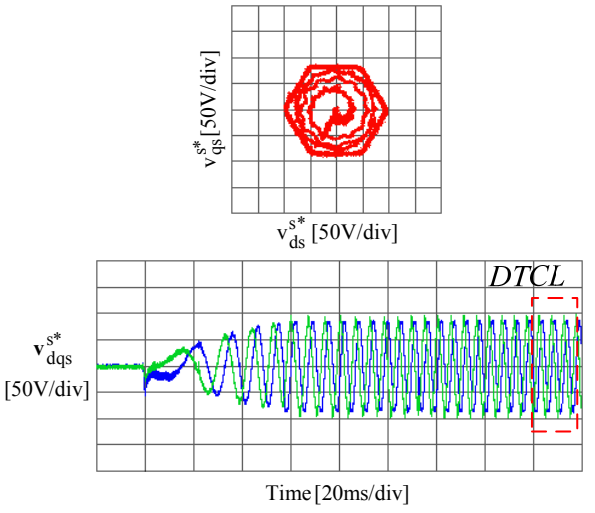

(a) Selected d-q command voltage waveforms.

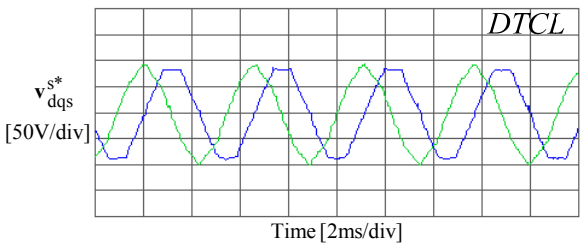

(b) Zoomed waveform of Fig. 11(a).

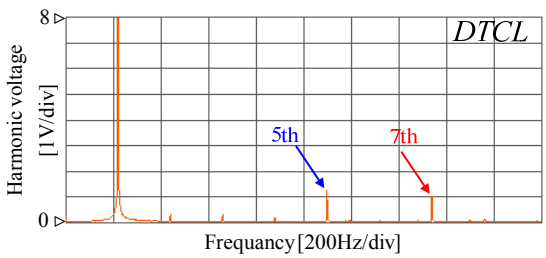

(c) FFT spectrum.

Fig. 11. Voltage waveforms of the DTCL-based FSS-DTFC.

The stator current is always bounded within I_{smax} in the FSS-DTFC mode, as illustrated in the bottom plot, because the enhanced FSS-DTFC works based on the discrete-time version of the current limit. This indicates that the developed voltage selection approach was successfully applied to the IPMSM with discrete-time physical limits. The resulting controller works reliably with the DB-DTFC and the proposed enhanced FSS-DTFC over the entire operating space.

Fig. 10 shows a spectral comparison of the d-q axis voltage command waveform of (5) in the stationary reference frame from starting to 3100 r/min. As mentioned above, the SSCL-based DTFC gives command voltage distortions with multiples of six times the fundamental frequency. These add-on harmonics may create unnecessary losses and can lead to mechanical vibrations.

Fig. 11 shows the selected d-q command voltage waveform of (11) from starting to 3100 r/min. In the SSCL-based FSS-DTFC, the magnitudes of the 5-th and 7-th components are 5 and 3 V, respectively, while those of the proposed method are less than 1 V. On the other hand, the fundamental component amplitude increases in the DTCL-based FSS-DTFC. The unbalanced component and the low-order harmonics observed in the SSCL-based DTFC were reduced remarkably because the proposed intersection stays in a considerably low fluctuation interval. In the proposed FSS-DTFC, the magnitudes of the 5-th and 7-th components are less than 1 V, while those of the SSCL-based FSS-DTFC are 5 and 3 V, respectively. On the other hand, the fundamental component amplitude increases in the proposed method. This can be confirmed from the x-y locus, where the resulting controller remains within the maximum voltage bound in the voltage limited condition.

TABLE I
RATINGS AND KNOWN PARAMETERS OF 900W IPMSM

Ratings and Parameters	Value	Unit
Rated torque	2.9	Nm
Number of poles	8	
Base speed@150 V_{dc}	1300	r/min
L_d	8.5	mH
L_q	20.2	mH
λ_{pm}	0.115	Wb

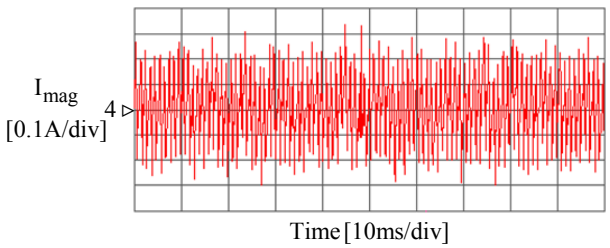

(a) SSCL-based FSS-DTFC.

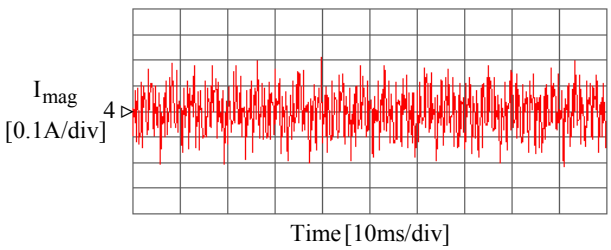

(b) Enhanced FSS-DTFC with the measured current.

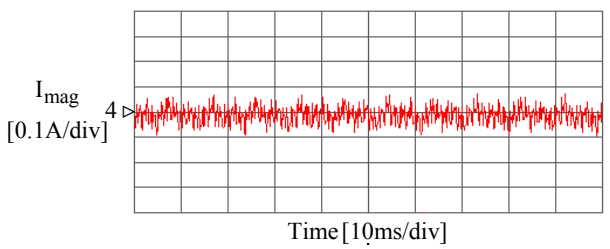

(c) Enhanced FSS-DTFC using the estimated current.

Fig. 12. Comparison of the stator current magnitude.

To assess how the proposed controller binds the stator current within the prescribed inverter current limit, the stator current magnitudes were compared, as shown in Fig. 12. Since it was contaminated by strong notching, the current signal in Fig. 12(a) was not sufficient to avoid instantaneous over-current. The irregular ripples associated with current measurement noise [see Fig 12(b)] are unsuitable for reliable current restrictions. On the other hand, when a properly estimated current is utilized, as shown in Fig. 12(c), the system achieves a stable response with a minimum amount of spike in the presence of sampled noise. This makes the proposed algorithm quite promising for inverter designs operating at various voltage limits.

V. CONCLUSIONS

The major contribution of this work is the development of a method to compute real time physical constraints for IPMSMs during voltage-limited operation. The enhanced version of the SSCL-based DTFC method makes a discrete time current limit to facilitate optimal voltage vector choices. The algorithm has the advantages of providing adequate results over a number of potential secondary upsets of a SSCL-based DTFC. The proposed control law dynamically scales the voltage vectors on the hexagonal voltage boundary based on a discrete-time version of the physical constraints. The inverter voltage can be more fully utilized via the DTCL-based DTFC than with the SSCL-based DTFC. In addition to the stator flux linkage and torque observer, a closed loop stator current observer is essential for accurately tracking and estimating changes in current in each switching period. This analytical solution leads to optimal voltage modifications at each time step with respect to the available inverter voltage.

ACKNOWLEDGMENT

This work was supported by the National Research Foundation of Korea under Grant 2010-0028509 funded by the Korean government (Ministry of Science, ICT, and Future Planning).

REFERENCES

[1] B. H. Kenny and R. D. Lorenz, "Stator and rotor flux based deadbeat direct torque control of an induction machine," *IEEE Trans. Ind. Appl.*, Vol. 39, No. 4, pp. 1093-1101, Jul./Aug. 2003.

[2] J. S. Lee, R. D. Lorenz, and M. A. Valenzuela, "Time-optimal and loss-minimizing deadbeat-direct torque and flux control for interior permanent-magnet synchronous machines," *IEEE Trans. Ind. Appl.*, Vol. 50, No. 3, pp. 1749-1758, May/Jun. 2014.

[3] I. Boldea, M. C. Paicu, G. D. Andreescu, and F. Blaabjerg, "Active flux DTFC-SVM sensorless control of IPMSM," *IEEE Trans. Energy Convers.*, Vol. 24, No. 2, pp. 314-322, Jun. 2009.

[4] J. S. Lee, C. H. Choi, J. K. Seok, and R. D. Lorenz, "Deadbeat direct torque and flux control of interior permanent magnet machines with discrete time stator current and stator flux linkage observer," *IEEE Trans. Ind. Appl.*, Vol. 47, No. 4, pp. 1749-1758, Jul./Aug. 2011.

[5] C. H. Choi, J. K. Seok, and R. D. Lorenz, "Wide-speed direct torque and flux control for interior PM synchronous motors operating at voltage and current limits," *IEEE Trans. Ind. Appl.*, Vol. 49, No. 1, pp. 109-117, Jan./Feb. 2013.

[6] S. H. Kim and J. K. Seok, "Finite-settling steps direct torque and flux control (FSS-DTFC) for torque-controlled interior PM motors at voltage limits," *IEEE Trans. Ind. Appl.*, Vol. 50, No. 5, pp. 3374-3381, Sep./Oct. 2014.

[7] S. H. Kim, C. H. Choi, and J. K. Seok, "Discrete-time physical limits-based enhanced finite-settling-step direct

torque and flux control for IPMSM drives," in *Proc. IEEE Energy Convers. Congr. Expo. Conf.*, pp. 1794-1800, 2013.
[8] G. Foo and M. F. Rahman, "Sensorless direct torque and flux-controlled IPM synchronous motor drive at very low speed without signal injection," *IEEE Trans. Ind. Electron.*, Vol. 57, No. 1, pp. 395-403, Jan. 2010.
[9] S. H. Kim and J. K. Seok, "Maximum voltage utilization of IPMSMs using modulating voltage scalability for automotive applications," *IEEE Trans. Power Electron*, Vol. 28, No. 124, pp. 5639-5646, Dec. 2013.
[10] R. L. Shrestha and J. K. Seok, "Online compensation of parameter variation effects for robust interior PM synchronous motor drives," *Journal of Power Electronics*, Vol. 11, No. 5, pp.713-718, Sep. 2011.

Sehwan Kim received his B.S. degree from Yeungnam University, Gyeongsan, Korea, in 2010, where he is presently working towards his combined M.S./Ph.D. degree in the Power Conversion Laboratory. His current research interests include high performance electrical machine drives, battery voltage maximum utilization for EVs/HEVs, and precise torque control of PM synchronous motors.

Jul-Ki Seok received his B.S., M.S., and Ph.D. degrees from Seoul National University, Seoul, Korea, in 1992, 1994, and 1998, respectively, all in Electrical Engineering. From 1998 to 2001, he was a Senior Engineer in the Production Engineering Center, Samsung Electronics, Suwon, Korea. Since 2001, he has been a faculty member in the School of Electrical Engineering, Yeungnam University, Gyeongsan, Korea, where he is presently working as a Professor. His current research interests include motor drives, power converter control of offshore wind farms, and nonlinear system identification related to the power electronics field. Dr. Seok was the recipient of the *IEEE Transactions on Industry Applications* Second Place Prize Paper Award, and is serving as an Associate Editor of the *IEEE Transactions on Industry Applications*.